Artifact-free balanced detection for the measurement of circular dichroism with a sub-picosecond time resolution

Pascale Changenet, François Hache

Artifact-free balanced detection for the measurement of circular dichroism with a sub-picosecond time resolution

PASCALE CHANGENET,[1*] AND FRANÇOIS HACHE[1]

[1]*Laboratoire d'Optique et Biosciences, CNRS, INSERM, École Polytechnique, Institut Polytechnique de Paris, Palaiseau 91128, France*
**pascale.changenet-barret@polytechnique.edu*

Abstract: Here we present the development of a subpicosecond spectropolarimeter enabling high sensitivity balanced detection of time-resolved circular dichroism (TRCD) signals from chiral sample in solution. The signals are measured with a conventional femtosecond pump-probe set-up using the combination of a quarter-waveplate and a Wollaston prism. This simple and robust method allows access to TRCD signals with improved signal-to-noise ratio and very short acquisition times. We provide a theoretical analysis of the artifacts of such detection geometry and the strategy to eliminate them. We illustrate the potential of this new detection with the study of the $[Ru(phen)_3]\cdot 2PF_6$ complexes in acetonitrile.

1. Introduction

Circular dichroism (CD) spectroscopy, which is the differential absorbance between left- and right-circularly polarized light, has become a tool of choice for studying the conformation of biomolecules at equilibrium in solution, under physiological conditions. Biomolecules exhibit characteristic CD signals in the ultraviolet (UV) spectral region between 200 and 300 nm that can be theoretically or phenomenologically related to their secondary structures [1]. In this context, transposition of CD measurements to the time domain (TRCD), in the UV-visible spectral domain, is a very promising strategy to access the conformational dynamics of proteins and oligonucleotides outside equilibrium that play a key role in their function. In this regard, the combination of CD detection and femtosecond pump-probe spectroscopy offers the possibility to access those dynamics over an extended time scale, ranging from femtoseconds to milliseconds, with a table top set-up.

Despite the conceptual simplicity of TRCD measurements, their implementation on conventional pump-probe setups remains an experimental challenge due to their very weak signals (*i.e.* 10^{-5}-10^{-3} in differential absorbance) subject to pump polarization artifacts [2]. Only a few groups have developed ultrafast TRCD setups in the UV-visible range (for a review, see [3, 4]). To date, only two types of detections have allowed for the comprehensive study of chiral compounds in solution [5-15]. The first one consists of direct TRCD measurements of the pump-induced differential absorbance variation of an alternately left- and right-circularly polarized probe [5, 8, 12, 13], while the second one relies on the measurement of the pump-induced ellipticity variation of a linearly polarized probe [14]. The main drawback of direct TRCD measurements stems from the detection of small absorbance changes against a strong achiral absorption background that significantly reduces their signal-to-noise (S/N) ratio. In contrast, background-free ellipticity measurements provide an enhanced detection of very small TRCD signals at a cost of an increased sensitivity to pump-induced linear birefringence (LB) artifacts due to their crossed-polarizer detection configuration [2, 16]. In addition, these two detection strategies require either the introduction of a modulation of the circularly polarized probe associated with a complex detection procedure to extract the TRCD signals [13], or of a

variable phase delay on the linearly polarized probe for each pump-probe delay which significantly increases the acquisition times [14]. These sequential acquisition procedures are very sensitive to pump and probe fluctuations which significantly reduces their S/N ratio.

Here, we specifically address these main drawbacks with the development of an alternative detection method based on the balanced detection of the pump-induced ellipticity changes of the probe linear polarization by chiral samples. The principle relies on the full characterization of the probe elliptic polarization with a single laser shot by using the combination of a broadband quarter-waveplate (QWP) and a Wollaston prism. In the following, we describe the principle and the implementation of this two-arm detection on a conventional single-wavelength detection femtosecond pump-probe set-up powered by a 1-kHz amplified Titanium Sapphire laser source. We perform a theoretical analysis of the artifacts for such detection geometry and provide a strategy to perform artifact-free TRCD measurements. We then illustrate the performances of our new set-up with the experimental study of $[Ru(phen)_3]\cdot 2PF_6$ complexes in acetonitrile.

2. Basic principle of TRCD with a balanced detection geometry

Taking advantage that the transmission of a linearly polarized light by a chiral medium is elliptical, the vertical and horizontal components of the ellipse can be directly accessed with the combination of a QWP and a Wollaston prism, as illustrated on Fig. 1 [4].

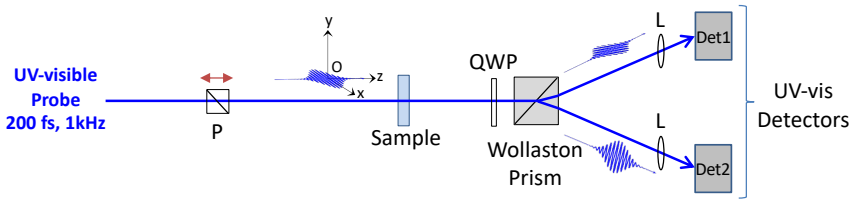

Fig. 1. Principle of single-shot balanced ellipsometry for a horizontally polarized incoming probe laser field along the (Ox) axis. P: Glan polarizer. QWP: quarter-waveplate. L: Lens. Det1and Det2: sample probe detectors (photodiodes or photomultipliers).

The effect of the different optical components on the incident probe polarized laser electric field can be described by the Jones formalism. The Jones vector for the horizontally polarized incoming probe light along the (Ox) axis is given by:

$$E^{in}=E_0 \begin{bmatrix}1\\0\end{bmatrix} \quad (1)$$

The outcoming probe laser field reads as:

$$E^{out} = M_{QWP} \cdot M_{sample} \cdot E^{in} \quad (2)$$

Each optical element is described by (2×2) matrix. The Jones matrix associated with the QWP, for an orientation at an angle of +45° (clockwise) with respect to its fast axis oriented along (Ox), is expressed as follows:

$$M_{QWP}^{45°} = \frac{1}{\sqrt{2}} \begin{bmatrix}1 & i\\ i & 1\end{bmatrix} \quad (3)$$

Chiral samples exhibiting small optical activity can be described with the Jones matrix [14]:

(4)

$$M_{sample}^{CD,CB} = e^{i\frac{2\pi}{\lambda}nL-\frac{\alpha L}{2}} \begin{bmatrix} 1 & i(i\theta+\gamma) \\ -i(i\theta+\gamma) & 1 \end{bmatrix} \quad (4)$$

where L is the sample thickness, n, the refractive index and α, the sample absorption coefficient. 4γ corresponds to the sample CD and θ to sample circular birefringence (CB), respectively defined as:

$$4\gamma = \ln(10) \cdot [A_L - A_R] \quad (5)$$

$$\theta = \pi \cdot \frac{n_L - n_R}{\lambda} \cdot L \quad (6)$$

where $A_{L,R}$ and $n_{L,R}$ are the sample absorbance and refractive index for left- and right-circularly polarized light. The outcoming laser probe field, for the QWP orientation at +45°, becomes:

$$E_{45°}^{out} = \frac{1}{\sqrt{2}} \cdot E_0 \cdot e^{i\frac{2\pi}{\lambda}nL-\frac{\alpha L}{2}} \begin{bmatrix} 1+\gamma+i\theta \\ i(1-(\gamma+i\theta)) \end{bmatrix} \quad (7)$$

The Wollaston prism then separates the output probe beam into two orthogonal polarizations. Their intensities measured with Det1 and Det2 (see Fig. 1) are respectively:

$$I_{45° Det1}^{out} = E_{x\,45°}^{out} \cdot \overline{E_{x\,45°}^{out}} = \frac{1}{2} \cdot {E_0}^2 \cdot e^{-\alpha L}(1+2\gamma+\gamma^2+\theta^2)$$
$$I_{45° Det2}^{out} = E_{y\,45°}^{out} \cdot \overline{E_{y\,45°}^{out}} = \frac{1}{2} \cdot {E_0}^2 \cdot e^{-\alpha L}(1-2\gamma+\gamma^2+\theta^2) \quad (8)$$

Neglecting the second order terms, γ^2 and θ^2 associated to the sample CD and CB that are <<1, static CD signals can be measured as follow:

$$S_{45°}^0 = 2 \cdot \frac{I_{45° Det1}^{out} - I_{45° Det2}^{out}}{I_{45° Det1}^{out} + I_{45° Det2}^{out}} = 4\gamma \quad (9)$$

It is interesting to note that with this detection geometry, CB does not contribute to the measured signals at first order. A similar result with opposite sign can be obtained for measurements performed for a QWP orientation at -45° (anti-clockwise) with respect to its fast axis (Ox):

$$S_{-45°}^0 = 2 \cdot \frac{I_{-45° Det1}^{out} - I_{-45° Det2}^{out}}{I_{-45° Det1}^{out} + I_{-45° Det2}^{out}} = -4\gamma \quad (10)$$

With the pump, the intensities of the two probe orthogonal polarizations measured with Det1 and Det2 (see Fig.1), for a QWP orientation at +45°, become:

$$I_{45° Det1}^{out\,pump} = \frac{1}{2} \cdot {E_0}^2 \cdot e^{-(\alpha+\Delta\alpha)L}[1+2(\gamma+\Delta\gamma)]$$
$$I_{45° Det2}^{out\,pump} = \frac{1}{2} \cdot {E_0}^2 \cdot e^{-(\alpha+\Delta\alpha)L}[1-2(\gamma+\Delta\gamma)] \quad (11)$$

with $\Delta\alpha$ and $4\Delta\gamma$, the pump-induced variations of the sample absorption coefficient and CD, respectively.

Measurements with the pump lead to:

$$S_{45°}^{pump} = 2 \cdot \frac{I_{45° Det1}^{out\ pump} - I_{45° Det2}^{out\ pump}}{I_{45° Det1}^{out\ pump} + I_{45° Det2}^{out\ pump}} = 4(\gamma + \Delta\gamma) \quad (12)$$

The differential TRCD signals can be retrieved by calculating the difference between the signals measured with the pump ($S_{45°}^{pump}$) and without the pump ($S_{45°}^{0}$), respectively:

$$S_{45°} = S_{45°}^{pump} - S_{45°}^{0} = 4\Delta\gamma \quad (13)$$

Similarly, we obtain for the TRCD measurements performed for a QWP orientation at -45°:

$$S_{-45°} = S_{-45°}^{pump} - S_{-45°}^{0} = -4\Delta\gamma \quad (14)$$

It should be stressed that the combination of the QWP and the Wollaston prism which separates the two circularly-polarized components of the transmitted probe, leads to the detection of two signals of nearly equal intensity in a balanced detection geometry. The measured differential signals thus give directly access to the CD variations of the sample (see Eqs. 13-14). This differs from the balanced heterodyne detection previously developed by Ghosh et *al.* for the measurement of the optical activity in the visible and near infrared spectral range, which consists in projecting into two equal intensities the transmitted probe electric field on an analog balanced photodetector with a Wollaston prism oriented at 45° [17]. With this geometry, both CD and CB signals contribute to the measured differential signals. A common-path interferometer is used to introduce a variable delay between the two projected probe polarizations to simultaneously recover the time-domain interferograms of these two contributions. Although proofs of principle for the measurement of the CD and CB spectra of chiral compounds in their ground electronic state have been given, it has not yet found application for ultrafast TRCD measurements [17]. It is worth noting that, despite this balanced heterodyne detection has the great advantage to give access to the whole CD and CB spectra of the sample with a simple set-up, its sequential acquisition procedure is expected to increase considerably the acquisition times in a pump-probe geometry. One main advantage of using the combination of the QWP and the Wollaston prism is to allow the characterization of the CD signals with a single laser shot. Such dual-arm detection geometry, which can be classified as a *non-null* ellipsometer, is commonly used in division-of-amplitude photopolarimeter (DOAP) for Mueller-matrix polarimetry [18]. Similar detection geometry combining a QWP and a polarization beam splitter has been also used for fast and improved S/N measurements of Raman optical activity (ROA) and circularly polarized luminescence (CPL) [19-22]. Here, this is the first implementation of such dual-arm *non-null* ellipsometry detection on a femtosecond pump-probe set-up. This differs from previously developed UV-visible ellipsometric TRCD detections, which were all based on conventional *quasi-null* ellipsometric detection methods[14, 23-25].

3. Theoretical analysis of TRCD balanced detection artifacts

Our previous analysis is valid for set-ups devoid of polarization artifacts. However, cross polarizer detection geometry is known to be particularly sensitive to pump-induced polarization artifacts and the sample cell window strain. Those artifacts have been already discussed in details by Kliger et al., in the frame of the development of nanosecond-millisecond ellipsometry, with a modified flash photolysis set-up [2]. Here, additional artifacts arising specifically from the balanced detection geometry must be considered. In the following, for simplicity, we discuss all these artifacts individually. In the experimental section, we provide evidence that these artifacts do not couple and can be individually corrected.

3.1 Pump-induced polarization artifacts

TRCD measurements with a cross-polarizer geometry are known to be very sensitive to artifacts stemming from the partial orientation of molecules excited with a linearly polarized pump [2, 14, 16]. This anisotropic effect creates sample LB and LD that can lead to strong artifacts in the TRCD signals, on the time scale of the rotational diffusion of the excited molecules. Correction of these artifacts is therefore crucial for measurements carried on the femtosecond time scale, notably for biomolecules that slowly reorient. We can evaluate these artifacts by considering the total sample matrix that contains the optical effects of the pump-induced LB and LD, in addition to the sample CD and CB, as previously defined by Xie et al. [26], expressed as:

(15)

$$M_{sample}^{CD,CB,LB,LD} = e^{i\frac{2\pi}{\lambda}(n+\Delta n)\cdot L-\frac{(\alpha+\Delta\alpha)L}{2}} \times \begin{bmatrix} 1-(ig+\beta)\cos(2\phi) & i(\gamma+\Delta\gamma)-(\theta+\Delta\theta)-(ig+\beta)\sin(2\phi) \\ -i(\gamma+\Delta\gamma)+(\theta+\Delta\theta)-(ig+\beta)\sin(2\phi) & 1+(ig+\beta)\cos(2\phi) \end{bmatrix}$$

where ϕ is the angle between the pump and probe linear polarizations, 4β and g are the sample LD and LB, respectively, defined as:

(16)

$$4\beta = \frac{A_x - A_y}{\ln(10)}$$

(17)

$$g = \pi \cdot \frac{n_y - n_x}{\lambda} \cdot L$$

where $A_{x,y}$ and $n_{x,y}$ are the absorbance and the refractive index along the (Ox) and (Oy) axes, respectively.

At first order (for the details of the calculation, see SI Eqs. S14-19), the TRCD signals measured for the two QWP orientations at ±45° read as:

(18)

$$S_{\pm 45^\circ} = \pm 4\Delta\gamma \pm 4g \cdot \sin(2\phi)$$

This result shows that the TRCD measurements at first order are not sensitive to the pump-induced LD. However, they can be strongly affected by the pump-induced LB, if the angle of the pump and probe linear polarizations slightly deviates from 0° or 90°. Note that this is particularly pernicious since it leads to an antisymmetric artefactual contribution to the TRCD signals measured for the two QWP orientations that cannot be corrected. In this regard, *in situ* alignment of the pump and probe polarizations with a precision of less than 1° has proven to be particularly effective to avoid pump-induced LB for quasi-colinear pump-probe configurations such as ours [27].

3.2 Sample cell birefringence artifact

Sample cell strain birefringence is known as one of the major drawbacks in ellipsometry. Effects of a small birefringence from the front or the back cell window can be modeled with the Jones matrix [14]:

(19)

$$M_{Cell}^{LB} = \begin{bmatrix} 1 & 2ib\psi \\ 2ib\psi & 1 \end{bmatrix}$$

where ψ is the angle between the fast axis of the birefringent window with respect to the probe polarization and 2b is the retardation. Taking into account the effect of the front cell window

LB, the measured CD signals without the pump, at first order for the QWP orientations at ±45°, express as (for the details, see SI Eqs. S10-15):

$$S^0_{\pm 45^\circ} = \pm 4\gamma \mp 8b\psi \quad (20)$$

From this calculation, it is clear that sample cell LB acts as a phase retarder which alters the elliptical probe eccentricity in the opposite directions on each detection arms. This leads to an antisymmetric artefactual contribution to the measured static CD signals for the two QWP orientations. Note that a similar effect is also expected from the back cell window. Importantly, the previous studies have shown that such artifact does not couple with the pump-induced artifacts, if the pump and probe polarizations are properly aligned [2]. Under these conditions, the sample cell LB is not expected to affect the TRCD signals. Those differential measurements fully cancel out this artefactual LB that contributes equally to the signals measured with and without the pump.

3.3 Unbalanced probe transmission artifacts

It is practically impossible to obtain a perfectly balanced detection due to the differences between the two detection arms. Notably, one of the main artifacts arises from the difference in the probe transmission, after the Wollaston prism, on the two detection arms due to their separate optics and detectors that may respond differently to the orthogonal polarizations of the probe. It is known from the previous developments of dual-arm detection for ROA and CPL that measurements performed for the two QWP orientations at ±45°, which inverts the two components of the elliptical probe polarization on the detection arms, can correct this problem [19]. This can be readily shown by calculating the CD signals for the two QWP orientations, taking into account the difference in the probe beam intensities transmitted on the two detection arms (for details, see SI Eqs. S16-22). This leads to CD signals that, at first order, are dissymmetric:

$$S^0_{\pm 45^\circ} = \pm 4\gamma + 2\Delta T \quad (21)$$

where ΔT is the normalized difference in the probe intensities transmitted on the two detection arms (T_{Det1} and T_{Det2}) expressed as:

$$\Delta T = \frac{T_{Det1} - T_{Det2}}{T_{Det1} + T_{Det2}} \quad (22)$$

This dissymmetry can be fully compensated by calculating the difference of the CD signals measured for these two QWP orientations:

$$\frac{1}{2} \cdot [S^0_{45^\circ} - S^0_{-45^\circ}] = 4\gamma \quad (23)$$

Importantly, the TRCD measurements, which are differential measurements with and without the pump are expected to fully compensate the ΔT dissymmetry, regardless of the QWP orientation.

3.4 Unbalanced probe separation artifacts

Another source of artifact of the balanced detection pertains from the unbalanced separation of the two probe linear polarizations upstream the Wollaston prism. This can be due to imperfection and/or misalignment of the QWP. Using the Jones formalism, a slight QWP misalignment from ±45° can be expressed as follows:

$$M_{QWP}^{X} = \begin{bmatrix} \cos(X) & i \cdot \sin(X) \\ i \cdot \sin(X) & \cos(X) \end{bmatrix} \quad (24)$$

with $X = \pm(45°+\delta)$ and δ, the angular deviation.

Unbalanced probe separation leads to dissymmetric CD signals for the two QWP orientations (for details, see SI Eqs. SI23-45):

$$S^{0}_{\pm(45°+\delta)} = \pm 4\gamma - 2\sin(2\delta) \quad (25)$$

Their difference allows to correct their dissymmetry:

$$\frac{1}{2} \cdot [S^{0}_{45°+\delta} - S^{0}_{-45°-\delta}] = 4\gamma \quad (26)$$

The situation is different for the TRCD measurements, for which the pump introduces additional sample LB. Thus, the unbalanced separation of the probe polarization not only affects the probe intensities, but also the amplitude of the transient absorption signals which is sent on the two detection arms. To evaluate such artefactual contributions, the total sample matrix that contains the optical effects of the pump-induced LB and LD, for parallel pump and probe polarizations, deduced from Eq. 15, as to be considered:

$$M_{sample}^{CD,CB,LB,LD} = e^{i\frac{2\pi}{\lambda}(n+\Delta n)\cdot L - \frac{(\alpha+\Delta\alpha)L}{2}} \times \begin{bmatrix} 1-(ig+\beta) & i(\gamma+\Delta\gamma)-(\theta+\Delta\theta) \\ -i(\gamma+\Delta\gamma)+(\theta+\Delta\theta) & 1+(ig+\beta) \end{bmatrix} \quad (27)$$

where 4β and g are the sample LB and LD (Eqs. 16 and 17), respectively.

For achiral samples (*i.e.* $\gamma = 0$, $\Delta\gamma = 0$, $\theta = 0$ and $\Delta\theta = 0$), the measured TRCD signals at first order, for the two QWP orientations are nonnull and read as:

$$S_{\pm(45°+\delta)} = 4\beta \cdot \sin(2\delta) \quad (28)$$

It is thus clear that the unbalanced separation of the probe, in the presence of the pump, induces the coupling of the TRCD signals with the pump-induced sample LD. This leads to the observation of the same artefactual TRCD signal for both QWP orientations, which yields:

$$\frac{1}{2} \cdot [S_{45°+\delta} - S_{-45°-\delta}] = 0 \quad (29)$$

In a similar way, we can show that chiral samples exhibit dissymmetric TRCD signals for the two QWP orientations:

$$S_{\pm(45°+\delta)} = \pm 4\Delta\gamma + 4\beta \cdot \sin(2\delta) \quad (30)$$

Their difference yields TRCD signals free from artifacts:

$$\frac{1}{2} \cdot [S_{45°+\delta} - S_{-45°-\delta}] = 4\Delta\gamma \quad (31)$$

4. Experimental set-up and processing

Time-resolved experiments are carried out with a single-wavelength detection pump-probe set-up using an amplified 1 kHz Ti:sapphire laser system (Spectra-Physics, Solstice), delivering 100-fs pulses at 800 nm with an energy of 3 mJ. The 400-nm pump pulses are obtained from the second harmonic of the fundamental pulses. Their energy is set to 0.37 μJ to avoid photo-degradation during experiments. Probe pulses at 270 nm with an energy of 12 nJ are generated by parametric amplification of a white light continuum and second harmonic generation.

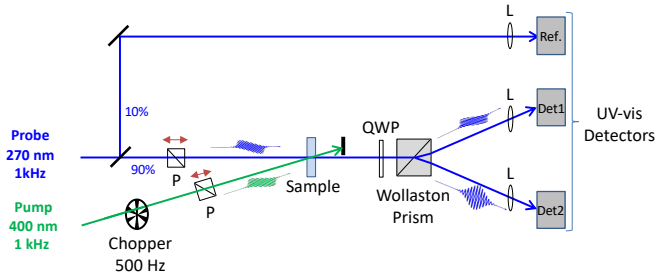

Fig. 2. Single-wavelength detection pump-probe set-up with a balanced ellipsometric TRCD detection. P: Glan polarizer. QWP: quarter-waveplate L: Lens. Det1and Det2: sample probe polarization detectors. Ref: reference probe detector.

Fig.2 illustrates the experimental set-up used for the balanced TRCD detection. The UV probe beam is split into the reference (10%) and the sample probe (90%) beams. The reference beam is directly sent to a variable gain photodiode (PDA25K2, Thorlabs) connected to a boxcar integrator (SR250, Standord Research Systems). The sample probe is focused into the sample cell with a typical diameter of about 400 μm, after passing through a Glan α-BBO polarizer (extinction ratio 10^5, Thorlabs) in order to get a horizontal polarization. The delay between the pump and probe beams is varied using an optical delay line driven by a stepper motor. TRCD measurements are performed by measuring the pump-induced ellipticity change of the sample probe beam with the combination of a broadband QWP (260-410 nm, Thorlabs) and a α-BBO Wollaston prism (extinction ratio 10^5, Thorlabs). The two probe beams are then sent through a set of identical mirrors, lenses and filters on two variable gain photodiodes connected to two boxcar integrators triggered with the TTL synchronization signal of the laser source regenerative amplifier and a 16-bits data acquisition card (National Instruments). Of note analog balanced photodetectors with sensitivity in the spectral range below 300 nm being not commercially available, we choose to use two variable gain photodiodes with an enhanced sensitivity between 150 and 550 nm.

The TRCD signals are measured by alternating measurements of the probe beam intensity of "pumped" and "unpumped" sample, the pump being modulated by a chopper at 500 Hz. Measured TRCD signals, for the two QWP angles at ±45° with respect to its fast axis, are averaged over 100 or 250 laser shots with the pump to reach an optimum S/N ratio. In a similar way, measured static CD signals are averaged over 100 or 250 laser shots without the pump. Importantly, in order to avoid interference from pump scattered light with the TRCD measurements, one UV bandpass filter (UG11) is added in front of each detector. The pump linear polarization is set to a parallel orientation with respect to the probe polarization with a Glan-Taylor calcite polarizer (extinction ratio 10^5, Thorlabs), in order to avoid pump-induced LB effects. The angles of the pump polarizer and the QWP are controlled with stepped-motorized rotation stages with a precision of $< 0.1°$. Fig.3 illustrates the measurements performed with Det1 and Det2, for various QWP angles. As shown by Fig.3, the intensities measured with Det1 and Det2 for the QWP orientations at +45° and +135° slightly differ by

ca. 5% (ΔT). This dissymmetry results from a combined effect of the unbalanced separation and transmission of the probe on the two detection arms.

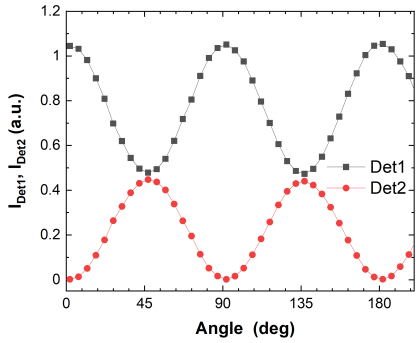

Fig. 3. Measured intensities averaged over 100 laser shots measured at 270 nm with the two detectors of the balanced ellipsometric TRCD detection. Det1 for the horizontal probe polarization and Det2 for the vertical probe polarization.

We find the ellipticity of the probe beam field equal to: $e = \sqrt{\frac{I_{min}}{I_{max}}} = 0.02$

In the following, we denote CD = 4γ/ln(10) and ΔCD = 4Δγ/ln(10), the steady-state and the transient CD signals, respectively. A = αL/ln(10) and ΔA = ΔαL/ln(10) are the sample absorbance and differential absorbance. The achiral differential ΔA signals are obtained simultaneously with the TRCD signals. In practice, for the QWP oriented at ±45°, the differential achiral absorbance signals are calculated from the averaged intensities measured on the three photodiodes (Det1, Det2 and Ref.) with a home-made program as follow:

(32)

$$\Delta A_{\pm 45^\circ} = -\log\left[\frac{I^{\text{out pump}}_{\pm 45^\circ\,\text{Det1}}}{I^{\text{out}}_{\pm 45^\circ\,\text{Det1}}} \times \frac{I^{\text{ref}}_{\pm 45^\circ}}{I^{\text{ref pump}}_{\pm 45^\circ}}\right] - \log\left[\frac{I^{\text{out pump}}_{\pm 45^\circ\,\text{Det2}}}{I^{\text{out}}_{\pm 45^\circ\,\text{Det2}}} \times \frac{I^{\text{ref}}_{\pm 45^\circ}}{I^{\text{ref pump}}_{\pm 45^\circ}}\right]$$

and the TRCD signals as follows:

(33)

$$\Delta CD_{\pm 45^\circ} = \pm\left\{-\log\left[\frac{I^{\text{out pump}}_{\pm 45^\circ\,\text{Det1}}}{I^{\text{out}}_{\pm 45^\circ\,\text{Det1}}}\right] + \log\left[\frac{I^{\text{out pump}}_{\pm 45^\circ\,\text{Det2}}}{I^{\text{out}}_{\pm 45^\circ\,\text{Det2}}}\right]\right\}$$

which is equivalent to Eqs. 13 and 14. From these measurements performed for the two orientations of the QWP, at ±45°, we calculate:

(34)

$$\Delta A = \frac{1}{2}[\Delta A_{45^\circ} + \Delta A_{-45^\circ}]$$

(35)

$$\Delta CD = \frac{1}{2}[\Delta CD_{45^\circ} - \Delta CD_{-45^\circ}]$$

All measurements are performed in regular 1-mm optical path quartz cells for absorption (Hellma). In order to increase the S/N ratio of the CD and ΔCD signals, the cell is kept fixed during the measurements to avoid unwanted birefringence effects. The steady-state absorption and CD spectra of the samples are measured before and after each TRCD experiments, in order to check for any sample degradation, with, respectively, an UV-visible Agilent Cary 100 spectrophotometer and a J-1500 Jasco CD spectrophotometer. The measured ΔCD kinetics traces are fitted with a Levenberg-Marquardt non-linear fitting algorithm to a sum of

exponential functions convoluted with a Gaussian function representing the instrumental response function (IRF). The full width at half maximum (FWHM) of the Gaussian is found to be ~0.90 ps.

5. Experimental results and discussion

5.1 Static CD measurements

In order to evaluate the capabilities of our experimental set-up, we first carried out static CD measurements on solutions of $[Ru(phen)_3]\cdot 2PF_6$ complexes of the same concentrations. Fig.4. shows the CD spectra of the two enantiomers and their racemic mixture measured in acetonitrile with a commercial CD spectrometer with the corresponding absorption spectrum of Λ-$[Ru(phen)_3]^{2+}$. Due to the propeller-twist arrangement of their phenanthroline ligands, these ruthenium complexes display strong CD signals in the spectral region of their absorption between 230 nm and 330 nm.

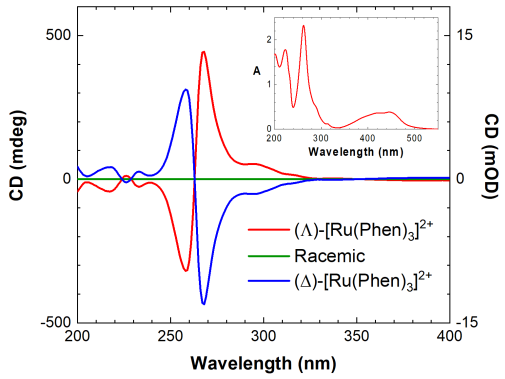

Fig. 4. Steady-state CD spectra of (Λ)-$[Ru(phen)_3]^{2+}$, (Δ)-$[Ru(phen)_3]^{2+}$ and their racemic mixture in acetonitrile measured with our commercial spectropolarimeter. Insert : Corresponding absorption spectrum of Λ-$[Ru(phen)_3]^{2+}$.

Table 1 gathers the static CD measurements carried out at 270 nm with our pump-probe set-up, for the two QWP orientations at ±45°, respectively. The CD signals retrieved from their difference (Eq. 23) and those measured with our commercial spectropolarimeter are also given for comparison. The CD measurements performed for the two QWP orientations all lead to negative values. Notably, we observe an offset of more than 40 mOD for the racemic mixture. These large offsets mainly arise from unbalanced detection artifacts (Eqs. 21 and 25) due to the differences in the transmission of the two probe polarizations on the two detection arms (ΔT=5%) in combination with the imperfect separation of their polarizations. Correction of these artifacts allow to obtain CD values of 16.4 and -8.2 mOD, for the Λ and Δ enantiomers of $[Ru(phen)3]^{2+}$ and -3.1 mOD for the racemic mixture. Although the sign and the order of magnitude of the CD signals of the two enantiomers are correct, they are highly dissymmetric. A significant offset from zero is also observed for the racemic mixture. Such a result is not surprising since the sample cell LB is not expected to cancel out for static CD measurements, as shown by the Jones calculations (Eq. 20).

Table 1. Static CD signals measured for solutions of $[Ru(phen)_3]\cdot 2PF_6$ complexes in acetonitrile at 270 nm with our balanced detection (ΔT~5%) averaged over 250 laser shots and our commercial spectropolarimeter. Given errors are the standard deviations of the measured signals.

	(Λ)-$[Ru(phen)_3]^{2+}$	Racemic mixture	(Δ)-$[Ru(phen)_3]^{2+}$
Measured signals	CD (mOD)	CD (mOD)	CD (mOD)
$\frac{1}{\ln(10)}\cdot S^0_{+45°}$	-27.7±0.4	-41.2±0.2	-54.6±0.3
$\frac{1}{\ln(10)}\cdot S^0_{-45°}$	-60.5±0.4	-47.5±0.2	-38.2±0.3
$\frac{1}{2\cdot\ln(10)}\cdot[S^0_{+45°}-S^0_{-45°}]$	16.4±0.8	-3.1±0.4	-8.2±0.6
Commercial spectro.	11.5	0.0	-11.2

Sample cell LB is known to lead to large offsets in the CD measurements [2]. Using our measurement of the racemic mixture as a baseline correction for the sample cell LB, we obtain CD values of 13 mOD and -11 mOD, respectively for the Λ and Δ enantiomers, which are much closer to those measured with our commercial spectropolarimeter (*i.e.* ±~11 mOD). Note, however, that the correction is not perfect, as a residual skewness of 2 mOD is still observed in the CD signals after the baseline subtraction. In fact, a similar result is obtained whether the measurements are performed in a single sample cell or three different cells. Therefore, under these experimental conditions, we deduce that the accuracy of the static CD measurements with our balanced detection geometry is limited to a few mOD. Different strategies can be considered to improve this accuracy, such as a careful alignment of the strained cells to reduce their LB and get Ψ~0 (Eq. 20) or the use of low-stress homemade sample cells. However, we show in the next section that this problem does not pose at all for the differential TRCD measurements, which allow to fully cancel out this LB artifact.

5.2 TRCD measurements

The TRCD signals are measured alternatively with and without the pump at a repetition rate of 1 kHz. Signals recorded at 270 nm, after excitation at 400 nm, lead to significant CD changes in the spectral region of the ππ* transition of the three ligands between 240 nm and 300 nm, the sign of which strongly depends on the wavelength [28]. The excitation of the lowest singlet excited state of $[Ru(phen)_3]^{2+}$ pertaining from the metal-to-ligand charge transfer (^{1}MLCT) state causes an ultrafast intersystem conversion in the sub-100-fs regime, leading to the formation of a long-lived triplet state (^{3}MLCT, $\tau \approx 0.6$ μs) with a quantum yield close to the unity [29]. The associated TRCD changes have been attributed to a change of the excitonic coupling between the ligands induced by the UV-visible excitation [28]. Note that electron localization/delocalization in the MLCT excited states of Ruthenium complexes is still a matter of debate (for review see [29]) and is not discussed further in this paper, which focuses on the experimental development of time-resolved ellipsometry.

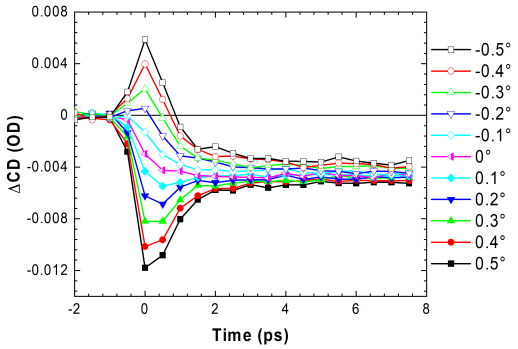

Fig. 5. ΔCD kinetic traces averaged over 100 laser shots measured for (Δ)-$[Ru(phen)_3]^{2+}$ in acetonitrile, at 270 nm, for different angles of the pump polarization with respect to the probe polarization, after excitation at 400 nm.

Fig.5. shows the ΔCD signals of (Δ)-$[Ru(phen)_3]^{2+}$ (Eq. 33) measured at 270 nm, for different angles of the pump polarization with respect to the probe polarization. The pump-induced LB leads to the observation of one antisymmetric peak around the time zero on the TRCD signals, as a function of the pump and probe polarization angle. This effect arises from the dependance of the TRCD signals with sin(2ϕ) (Eq. 18) and thus disappears when the pump and probe polarizations are aligned (ϕ=0). An alignment with a precision of 0.1° is found to properly eliminate the pump-induced LB (*i.e.* ΔCD <5 μOD, for the racemic mixture, for data acquisition over 500 laser shots). We found this alignment to be very robust to day-to day pump and probe alignment, as long as the angle of the input polarizer angle of the probe remains unchanged. Note that another strategy to eliminate the pump-induced LB would be to use depolarized pump pulses. However, generation of randomly polarized pump pulses with commercial depolarizers has proved ineffective to fully eliminate the pump-induced LB. An alternative strategy would be to use a common polarizer for the pump and probe, as previously done for subpicosecond ellipsometry with a Babinet-Soleil compensator [9, 10]. But under our current experimental conditions, this strategy has also proved ineffective to fully remove the pump-induced LB, probably because the polarizer has to be placed very close to the sample cell where the pump and probe beams are highly convergent.

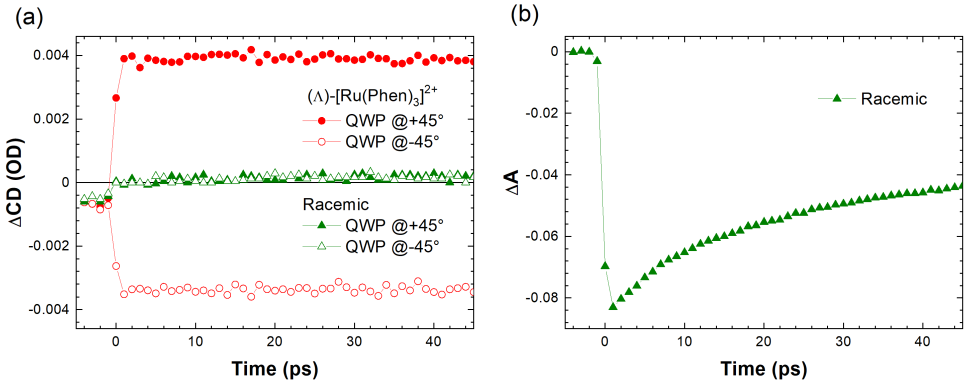

Fig. 6. (a) ΔCD kinetic traces averaged over 250 laser shots measured at 270 nm, after excitation at 400 nm, for (Λ)-$[Ru(phen)_3]^{2+}$ and the racemic mixture in acetonitrile, for a QWP orientation at +45° and -45°, respectively. ΔT= ca. 5%. (b) Corresponding ΔA kinetic trace measured for the racemic mixture.

The great advantage of the balanced detection is that it does not require any modulation of the probe polarization, avoiding complex synchronization procedures to extract the TRCD signals.

However, as shown by the Jones calculations, such a detection may lead to specific artifacts due to imperfect separation of the two probe polarizations. Fig. 6.a illustrates effects of these artifacts on the ΔCD signals of (Λ)-$[Ru(phen)_3]^{2+}$ and the racemic mixture measured for the two QWP orientations at +45° and -45°, respectively. It is worth noting that, in all cases, we observe residual negative signals on the order of $5x10^{-4}$ before the time zero. Origin of these signals has not been elucidated yet. We think they might stem from residual ΔA signals associated with the long-lived photoproduct that has not fully relaxed between two pump laser shots or residual sample pump scattering. In addition, as predicted by Eq. 30, imperfections of the balanced detection lead to the observation of dissymmetric ΔCD signals after the time zero, corresponding to an artefactual increase of the positive ΔCD signals and an attenuation of the negative ones. Concomitantly, the TRCD measurements performed on the racemic mixture exhibit small ΔCD signals after the time zero, that directly illustrates the imperfect separation of the achiral ΔA signals (Fig. 6b), as expected from Eq. 28. Importantly these artefactual signals before and after the time zero are found to be similar for the two QWP orientations and therefore can be easily removed by calculating their difference.

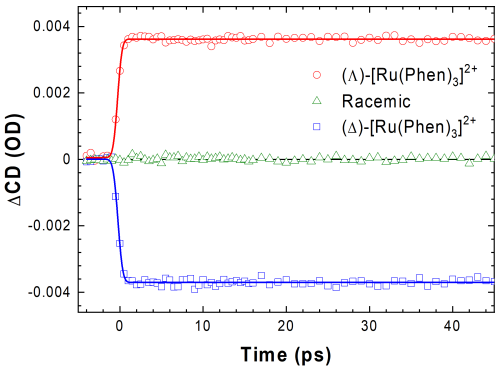

Fig. 7. ΔCD kinetic traces averaged over 500 laser shots measured for (Δ)-$[Ru(phen)_3]^{2+}$, (Λ)-$[Ru(phen)_3]^{2+}$ and their racemic mixture, in acetonitrile at 270 nm, after excitation at 400 nm and correction for unbalanced detection artifacts. Solid lines represent the individual fits of the experimental data.

This is illustrated on Fig.7 which displays the ΔCD signals measured for (Λ)-$[Ru(phen)_3]^{2+}$, (Δ)-$[Ru(phen)_3]^{2+}$ and their racemic mixture in acetonitrile, after correction for the unbalanced detection artifacts (Eqs. 29 and 331). The ΔCD signal of the racemic mixture leads to a mean value of -3 μOD (*i.e.* 0.1 mdeg) for data acquisitions over 500 laser shots. This result clearly shows that the TRCD measurements performed at the two QWP orientations can compensate for the imperfections of the balanced detection, before and after the time zero. Importantly, in contrast to static CD measurements, we do not observe any significant effect of the sample cell LB on the ΔCD signals of the two enantiomers, which are the mirror-image of each other. The observed changes in the ΔCD signals and their signs are consistent with an ultrafast (<100 fs) electronic relaxation pertaining from the intersystem conversion from the excited ^{1}MLCT state, which leads to a fast change of the CD in the excited state [28]. The associated ΔA changes are negative (see Fig. 6b), which indicate a dominant contribution of the ground state bleach arising from the ligand absorption band at 270 nm. In contrast to the ΔCD signals, which remain constant after excitation, the ΔA signals exhibit a 19-ps decay followed by a plateau. This decay time is comparable with the vibrational relaxation time of the formed ^{3}MLCT state previously reported by the studies of the $[Ru(bpy)_3]^{2+}$ complexes in acetonitrile studied by time-resolved resonance Raman spectroscopy and IR femtosecond spectroscopy [30, 31].

The fits of the ΔCD (Fig. 7) and ΔA kinetics (Fig. 6b) of the $[Ru(phen)_3]\cdot 2PF_6$ complexes allow to estimate the IRF of our TRCD set-up to 0.90 ± 0.05 ps. This spread of the IRF is essentially due to the dispersion of the pump and probe pulses in the high extinction coefficient polarization optics used to the precise control of their polarization. The fits allow to quantify the ΔCD changes of the two enantiomers to values of ±365 μOD. Thanks to the balanced detection geometry, the laser probe fluctuations can be substantially compensated, which leads to an accuracy on these TRCD measurements of 30 μOD, which is one order of magnitude higher than that of our referenced achiral transient absorption measurements (300 μOD) for data acquisition over 500 laser shots. This corresponds to an improvement by a factor 20 in the data acquisition times in comparison with our previous time-resolved ellipsometry set-up using a Babinet-Soleil compensator [14]. Typically, kinetics traces of Fig. 7 required acquisition times of a few minutes *vs.* a few hours with our previous set-up using a Babinet-Soleil compensator.

The present experimental results provide evidence that TRCD measurements performed for two QWP orientations, respectively at ±45°, fully correct artifacts inherent to the balanced detection (Eqs. 21-31) and pump-induced LB (Eqs. 15-18), when pump and probe polarizations are properly aligned. In addition, these differential measurements with and without the pump, overcome the polarization artifacts typically encountered in static ellipsometry (Eqs. 19-20), allowing artifact-free TRCD measurements to be performed in regular absorption cells. This is a significant improvement compared to previous TRCD setups that usually require the use of homemade weakly birefringent sample cells or even sample jets [2, 11, 14]. This also explains the better accuracy we obtain for the TRCD measurements *vs.* the static CD measurements with our balanced detection geometry. Thus, taken all together, these advantages allow us to propose a simple and robust experimental set-up without any polarization modulation to access artifact-free TRCD signals with a sub-picosecond time resolution.

6. Conclusion

We have described the first implementation of *non-null* ellipsometry with a balanced detection geometry on a classical femtosecond pump-probe setup. The great advantage of this simple detection geometry is that it does not require any polarization modulation, allowing subpicosecond TRCD measurements with very reduced acquisition times (*i.e.* over 500 laser shots) and an accuracy of 1 mdeg. Thanks to the rigorous control of the pump and probe linear polarizations, we demonstrated the feasibility of artifact-free TRCD measurements in regular quartz spectroscopic cells. These improvements represent an important technical progress opening the way for the development of more amenable TRCD detections on ultrafast pump-probe setups. One future challenge in the development of such a type of detection lies in the improvement of its temporal resolution with the use of less dispersive polarization optics and the pre-compensation of their chirp. A second challenge lies in the increase of the precision of the TRCD measurements. Notably with the use of a high repetition-rate femtosecond Ytterbium laser source as the probe, an accuracy of a few μOD in the TRCD measurements is expected to be easily reached.

Funding

This work was supported by the French national funding research agency (ANR):ANR-22-CE30-0001-01 ChirADASOPS) and the MITI CNRS call “Lumière et Vie 2022”.

Acknowledgments

The authors thank Baptiste Thiaudière (Paris Saclay Polytech internship) and Martha Yaghoubi Jouybari (European Training Program LightDyNamics) for their help in the development of the probe polarization measurements. Authors thank Marie Claire Schanne-Klein (Laboratoire

d'Optique et Biosciences, Palaiseau, France) for valuable scientific discussions for the redaction of this article.

Disclosures

The authors declare no conflicts of interest

Supplemental document

See Supplement 1 for supporting content.

Data availability

The data underlying the results presented herein are not publicly available currently but can be obtained from the authors upon reasonable request.

References

1. G. D. Fasman, *Circular dichroism and the conformational analysis of biomolecules* (Springer New York, NY, 2010).
2. S. C. Björling, R. A. Goldbeck, S. J. Milder, C. E. Randall, J. W. Lewis, and D. S. Kliger, "Analysis of optical artifacts In ellipsometric measurements of time-resolved circular dichroism," J. Phys. Chem. **95**, 4685 (1991).
3. F. Hache, and P. Changenet, "Multiscale conformational dynamics probed by time-resolved circular dichroism from seconds to picoseconds," Chirality **33**, 747 (2021).
4. P. Changenet, and F. Hache, "Recent advances in the development of ultrafast electronic circular dichroism for probing the conformational dynamics of biomolecules in solution," Eur. Phys. J. Spec. Top. **DOI: 10.1140/epjs/s11734-022-00679-3** (2022).
5. A. Trifonov, I. Buchvarov, A. Lohr, F. Würthhner, and T. Fiebig, "Broadband femtosecond circular dichroism spectrometer with white-light polarization control," Rev. Sci. Instrum. **81**, 043104 (2010).
6. T. Dartigalongue, C. Niezborala, and F. Hache, "Subpicosecond UV spectroscopy of carbonmonoxy-myoglobin: absorption and circular dichroism studies," Phys. Chem. Chem. Phys. **9**, 1611-1615 (2007).
7. F. Hache, M. Khuc, J. Brazard, P. Plaza, M. Martin, G. Checcucci, and F. Lenci, "Picosecond transient circular dichroism of the photoreceptor protein of the light-adapted form of Blepharisma japonicum," Chem. Phys. Lett. **483**, 133-137 (2009).
8. J. Meyer-Ilse, D. Akimov, and B. Dietzek, "Ultrafast circular dichroism study of the ring opening of 7-Dehydrocholesterol," J. Phys. Chem. Lett. **3**, 182-185 (2012).
9. L. Mendonca, F. Hache, P. Changenet-Barret, P. Plaza, H. Chosrowjan, S. Taniguchi, and Y. Imamoto, "Ultrafast carbonyl motion of the Photoactive Yellow Protein chromophore probed by femtosecond circular dichroism," J. Am. Chem. Soc. **135**, 14637-14643 (2013).
10. M. Schmid, L. Martinez-Fernandez, D. Markovitsi, F. Santoro, F. Hache, R. Improta, and P. Changenet, "Unveiling excited-state chirality of binaphthols by femtosecond circular dichroism and quantum chemical calculations," J. Phys. Chem. Lett. **10**, 4089-4094 (2019).
11. M. Oppermann, J. Spekowius, B. Bauer, R. Pfister, M. Chergui, and J. Helbing, "Broad-band ultraviolet CD spectroscopy of ultrafast peptide backbone conformational dynamics," J. Phys. Chem. Lett. **10**, 2700-2705 (2019).
12. M. Morgenroth, M. Scholz, T. Lenzer, and K. Oum, "Ultrafast UV-vis transient absorption and circular dichroism spectroscopy of a polyfluorene copolymer showing large chiral induction," J. Phys. Chem. C **124**, 10192-10200 (2020).
13. M. Oppermann, B. Bauer, T. Rossi, F. Zinna, J. Helbing, J. Lacour, and M. Chergui, "Ultrafast broadband circular dichroism in the deep ultraviolet," Optica **6**, 56 (2019).
14. C. Niezborala, and F. Hache, "Measuring the dynamics of circular dichroism in a pump-probe experiment with a Babinet-Soleil compensator," J. Opt. Soc. Am. B **23**, 2418-2424 (2006).

15. M. Oppermann, F. Zinna, J. Lacour, and M. Chergui, "Chiral control of spin-crossover dynamics in Fe(II) complexes," Nat. Chem. **14**, 739-745 (2022).
16. B. Dutta, and J. Helbing, "Optimized interferometric setup for chiral and achiral ultrafast IR spectroscopy," Opt. Express **23**, 16449 (2015).
17. S. Ghosh, G. Herink, A. Perri, F. Preda, C. Manzoni, D. Polli, and G. Cerullo, "Broadband optical activity spectroscopy with interferometric Fourier-transform balanced detection," ACS Photonics **8**, 2234-2242 (2021).
18. R. M. A. Azzam, "Stokes-vector and Mueller-matrix polarimetry," J. Opt. Soc. Am. A **33**, 1396-1408 (2016).
19. W. Hug, and G. Hangartner, "A novel high-throughput Raman spectrometer for polarization difference measurements," J. Raman Spectrosc. **30**, 841-852 (1999).
20. L. E. MacKenzie, L.-O. Pålsson, D. Parker, A. Beeby, and R. Pal, "Rapid time-resolved Circular Polarization Luminescence (CPL) emission spectroscopy," Nat. Commun. **11**, 1676 (2020).
21. F. Gendron, S. D. Pietro, L. A. Galán, F. Riobé, V. Placide, L. Guy, F. Zinna, L. D. Bari, A. Bensalah-Ledoux, Y. Guyot, G. Pilet, F. Pointillart, B. Baguenard, S. Guy, O. Cador, O. Maury, and B. L. Guennic, "Luminescence, chiroptical, magnetic and ab initio crystal-field characterizations of an enantiopure helicoidal Yb(III) complex," Inorg. Chem. Front. **8**, 914-926 (2021).
22. B. Baguenard, A. Bensalah-Ledoux, L. Guy, F. Riobe, O. Maury, and S. Guy, "Theoretical and experimental analysis of circularly polarized luminescence spectrophotometers for artifact-free measurements using a single CCD camera," Nat. Commun. **14**, 1065 (2023).
23. D. S. Kliger, and J. W. Lewis, "Recent advances in time resolved circular-dichroism spectroscopy," Rev. Chem. Intermed. **8**, 367-398 (1987).
24. L. Mangot, G. Taupier, M. Romeo, A. Boeglin, O. Cregut, and K. D. Dorkenoo, "Broadband transient dichroism spectroscopy in chiral molecules," Opt. Lett. **35**, 381-383 (2010).
25. K. Hiramatsu, and T. Nagata, "Broadband and ultrasensitive femtosecond time-resolved circular dichroism spectroscopy," J. Chem. Phys. **143**, 121102 (2015).
26. X. Xie, and J. D. Simon, "Picosecond circular dichroism spectroscopy: a Jones matrix analysis," J. Opt. Soc. Am. B **7**, 1673-1684 (1990).
27. C. M. Einterz, J. W. Lewis, S. J. Milder, and D. S. Kliger, "Birefringence effects in transient circular dichroism measurements with applications to the photolysis of carbon monoxyhemoglobin and carbon monoxymyoglobin," J. Phys. Chem. **89**, 3845-3853 (1985).
28. C. Niezborala, and F. Hache, "Excited-state absorption and circular dichroism of Ruthenium(II) Tris(phenanthroline) in the ultraviolet region," J. Phys. Chem. A **111**, 7732-7735 (2007).
29. P. Dongare, B. D. B. Myron, L. Wang, D. W. Thompson, and T. J. Meyer, "[Ru(bpy)3]2+* revisited. Is it localized or delocalized? How does it decay?," Coord. Chem. Rev. **345**, 86-107 (2017).
30. W. Henry, C. G. Coates, C. Brady, K. L. Ronayne, P. Matousek, M. Towrie, S. W. Botchway, A. W. Parker, J. G. Vos, W. R. Browne, and J. J. McGarvey, "The early picosecond photophysics of Ru(II) Polypyridyl complexes: a tale of two timescales," J. Phys. Chem. A, **112**, 4537-4544 (2008).
31. Q. Sun, B. Dereka, E. Vauthey, L. v. M. L. Daku, and A. Hauser, "Ultrafast transient IR spectroscopy and DFT calculations of ruthenium(II) polypyridyl complexes," Chem. Sci. **8**, 223-230 (2017).